

This work was written as part of one of the author's official duties as an Employee of the United States Government and is therefore a work of the United States Government. In accordance with 17 U.S.C. 105, no copyright protection is available for such works under U.S. Law.

Public Domain Mark 1.0

<https://creativecommons.org/publicdomain/mark/1.0/>

Access to this work was provided by the University of Maryland, Baltimore County (UMBC) ScholarWorks@UMBC digital repository on the Maryland Shared Open Access (MD-SOAR) platform.

Please provide feedback

Please support the ScholarWorks@UMBC repository by emailing scholarworks-group@umbc.edu and telling us what having access to this work means to you and why it's important to you. Thank you.

Changes in the Earth's UV reflectivity from the surface, clouds, and aerosols

J. R. Herman

Laboratory for Atmospheres, Goddard Space Flight Center, Greenbelt, Maryland

D. Larko

Raytheon STX Corporation, Lanham, Maryland

E. Celarier and J. Ziemke

Software Corporation of America, Beltsville, Maryland

Abstract. Measurements of the Earth's 380 nm UV reflectivity combine the effects of surface reflectivity, aerosols, haze, cloud optical thickness, and the fraction of the scene covered by clouds. Changes in UV cloud and aerosol reflectivity would imply similar changes over a wide range of wavelengths, UV, visible, and near infrared (at least 0.3 to 2 μm), affecting both the transmission of radiation to the Earth's surface and the reflection back to space. Using the TOMS (Total Ozone Mapping Spectrometer) 380 nm reflectivity data, the 14-year annual mean power reflected back to space is $385.3 \pm 31 \text{ W/m}^2$, mostly by clouds, aerosols, and snow/ice. On the basis of measured long-term changes in global reflectivity, it is estimated that there is an additional $2.8 \pm 2.8 \text{ W/m}^2$ per decade reflected back to space (2 standard deviation error estimate) during the TOMS observing period of 1979–1992. Since the 380 nm surface reflectivity is low (2–8%) over most surfaces, water and land, the observed reflectivity changes are mostly caused by changes in the amount of snow/ice, cloudiness, and aerosols. Time series analysis of TOMS reflectivity over the period from 1979 to 1992 shows that there were no significant changes in annually averaged zonal-average reflectivity at latitudes within 60°S–60°N, even though there were changes at higher latitudes (e.g., 3% per decade, in reflectivity units, between 60°N and 70°N). When the effects of the 11.3-year solar cycle and ENSO (El Niño–Southern Oscillation) are removed from the data, statistically significant reflectivity changes are observed poleward of both 40°S and 40°N. The presence of a statistically significant 11.3-year periodicity in the reflectivity time series correlates with the solar cycle and suggests a possible Sun-weather relationship. There are significant regional changes in reflectivity R over land and ocean areas that affect the amount of solar radiation reaching the surface. The largest of these regions have decreases in R of 3 to $6 \pm 1\%$ per decade in central Europe, the western United States, central China, and western Russia. These decreases are offset by increases in the same latitude bands mostly over the oceans. The largest regions showing an increase in R are off the western coast of South America (near Chile and Peru), 5 to $8 \pm 1\%$ /decade and over the Weddell Sea in Antarctica of 10%/decade, but no change over the ice shelf and continent. The largest increase in R occurs over the ocean just to the north of Antarctica. This change is important because it reduces UV radiation overall (290–400 nm) and partially offsets the effect of the increased amount of UV-B radiation (290–320 nm) caused by decreasing Antarctic ozone.

1. Introduction

Recent studies, based on TOMS (Total Ozone Mapping Spectrometer) estimates of UV changes over the period 1979–1992, suggested that there were no significant changes in the global or zonal average reflectivity for 380 nm radiation [Herman *et al.*, 1996; Lubin *et al.*, 1998] between $\pm 55^\circ$ latitude. Kuang *et al.* [1998], using International Satellite Cloud Climatology Project (ISCCP) data, have discussed the likelihood that global cloud fraction has increased at the same time that op-

tical depth has decreased in such a manner as to keep the reflectivity approximately constant. These estimates did not consider removal of solar cycle or El Niño–Southern Oscillation (ENSO) effects that partially mask small decadal reflectivity changes at midlatitudes. Studies of UV reflectivity are important because of the strong climate effect that could be caused by any global change in atmospheric reflectivity (reflectivity from the surface, clouds, and aerosols). Changes in UV cloud and aerosol reflectivity would imply similar changes over a wide range of wavelengths, UV, visible, and near infrared (at least 0.31–2 μm), affecting both the transmission of radiation to the Earth's surface and the reflection back to space.

This study will discuss the characteristics of the 14-year Nimbus-7/TOMS reflectivity time series, estimate long-term

Copyright 2001 by the American Geophysical Union.

Paper number 2000JD900435.
0148-0227/01/2000JD900435\$09.00

changes, globally, for zonal averages by month and year, and by geographic region. The reflectivity data set will be used to estimate the amount of solar energy (300–4000 nm) reflected back to space by clouds, aerosols, and snow/ice. In order to validate the use of TOMS data for estimation of changes in reflectivity, a demonstration of the long-term stability of the TOMS 380 nm measured reflectivity is given.

Use of TOMS UV (ultraviolet) radiance data for cloud reflectivity studies has an important advantage over longer-wavelength observations in the visible and infrared ranges, namely that the background is dark over land, vegetation, and water with a surface reflectivity always in the range of 2–8 RU (1 reflectivity unit RU = 1% reflectivity) [Eck et al., 1987; Herman and Celarier, 1997], except for some deserts and clear ocean water having reflectivities near 8 RU. At visible and near-IR wavelengths (400–4000 nm) there is a strong response to changes in vegetation. In the UV there is only a small seasonal variation in the 2–8 RU ocean reflectivity, partially caused by phytoplankton, and in the 2–4 RU ground reflectivity, caused by plant growth, except when there is snow or ice on the ground. The measured Lambert equivalent scene reflectivity is a combination of the underlying ground or ocean reflectivity, surface haze, and the reflectivity of clouds and aerosols within the TOMS field of view (FOV). Because of the large FOV from Nimbus 7/TOMS, 50 km × 50 km at nadir view and 100 km × 100 km average, only scene-average properties are measured instead of the much more complex properties of individual clouds or small groups of clouds. The details of the computation of scene reflectivity are given in other articles for a wide range of conditions over both land and oceans [Krotkov et al., 1998, 2000 (hereinafter referred to as K2000); Herman et al., 1999, 2000 (hereinafter referred to as H2000)].

When considering a large region (100 km × 100 km) containing clouds, the penetration of UV radiation through clouds, and the radiation reflected back to space, can be represented by tabulated solutions of the radiative transfer equation or, in a simpler manner, by an expression based on Lambert equivalent scene reflectivity R . To a first-order approximation the transmittance T_{CLOUD} of UV radiation to the ground, relative to that of a pure Rayleigh scattering atmosphere T_{CLEAR} , is given by [Eck et al., 1995] in terms of the measured scene reflectivity R and surface reflectivity R_s , where $R_s = 0.05$ and $0.05 \leq R \leq 1$,

$$C_T^{\text{ECK}} = T_{\text{CLOUD}}/T_{\text{CLEAR}} \approx \begin{cases} [1 - (R - R_s)/(1 - 2R_s)] & R \leq 0.5 \\ \approx 1 - R & R > 0.5. \end{cases} \quad (1)$$

More accurate approximations to C_T can differ from C_T^{ECK} by 40% depending on solar zenith angle, satellite zenith angle, and cloud optical depth but still depend most strongly on the value of $1 - R$ [Herman et al., 1999]. If data for a given location are averaged over several days, then the satellite zenith angle changes throughout its entire range. Under these circumstances, the accuracy of the average measured C_T^{ECK} relative to C_T is about 10%. Comparisons with ground-based data [Herman et al., 1999; Krotkov et al., 1998, K2000] suggest that the measured reflectivities from the TOMS FOV apply to the more general situation of mixed scenes containing clear-sky days, continuous-cloud days, and broken-cloud days when averaged over at least 1 week. For weekly averaged values the accuracy of C_T relative to ground-based estimates of the same quantity is about 3% when the ground-based measurements

are obtained within ± 2 hours of the satellite overpass time (K2000). The results show that the measured values of R are closely related to the average energy transmitted to the ground and energy reflected back to space.

The need for weekly averaging only applies to comparisons with ground-based measurements. The problem arises from the different fields of view. The TOMS FOV is about 100 km × 100 km, while the ground-based observation is viewing a much smaller region of the sky. At any given moment, the ground station could be viewing either clear sky or a cloud, while TOMS would be viewing the average for the FOV region surrounding the ground instrument. Time averaging allows the ground station to sample a larger area because of cloud motions and is likely to be more equivalent to the TOMS spatial sample.

A portion of the measured reflectivity is due to aerosols (nonabsorbing aerosols in the UV, haze, absorbing dust, smoke, or volcanic ash), which are frequently present in the TOMS FOV. The theoretical basis for the relationship between aerosol amounts and reflectivity has been given by Torres et al. [1998] and Krotkov et al. [1998]. The global distribution of these aerosols has been described by Herman et al. [1997] with local validation using ground-based data in the works of Hsu et al. [1999] and Chiapello et al. [1999]. Empirical relationships between satellite-measured aerosol characteristics and ground-based Sun-photometer-measured optical depths are given by Hsu et al. [1999] and Herman et al. [1999]. In general, smoke and nonabsorbing aerosols tend to increase the UV reflectivity in otherwise clear scenes by only a few percent, while dust and volcanic ash tend to decrease the UV reflectivity. Regions containing large amounts of dust or smoke (optical depths greater than 0.7) tend to cover about 10% of the Earth's surface (mostly in the latitude range $\pm 30^\circ$), while aerosol amounts of all types with small optical depths (0.2–0.5) have been observed at all latitudes between $\pm 65^\circ$. Absorbing aerosols may be present at higher latitudes, but the analysis has not been carried out for satellite data.

The 380 nm LER (Lambert equivalent reflectivity) is calculated by requiring that the measured TOMS radiance I_{SM} match the calculated radiance I_s (see equation (2)) by adjusting a single free parameter R in the formal solution of the radiative transfer equation

$$I_s(\Omega, \Theta, R, P_0) = \frac{RI_d(\Omega, \Theta, P_0)f(\Omega, P_0)}{1 - RS_b(\Omega, P_0)} + I_{a0}(\Omega, \Theta, P_0), \quad (2)$$

where

Θ = viewing geometry (solar zenith angle, satellite zenith angle, azimuth angle)

R = LER (the combined effect of the surface, clouds, water haze, and aerosols);

P_0 = reflecting surface pressure;

I_{a0} = radiance scattered back from the atmosphere for $R = 0$ and $0 < P < P_0$;

S_b = fraction scattered back to P_0 from the atmosphere;

I_d = sum of direct and diffuse radiation reaching P_0 ,

f = fraction of radiation reflected from P_0 reaching the satellite.

The resulting values of R represent the Lambert equivalent reflectivity (LER) of the scene from measured backscattered radiances originating from the ground, aerosols, and clouds as

components of the reflectivity. Certain scenes, such as those containing ice or specular reflection, are distinctly non-Lambertian (e.g., ocean Sun glint), as are clouds observed at large solar zenith angles. Since this study considers long-term changes in measured monthly-average reflectivity as from the Sun-synchronous TOMS polar orbit, only relative values are used, obtained at approximately constant-viewing angles for each region of the Earth for the same day of the year. This makes the long-term reflectivity-change estimates insensitive to the Lambertian reflectivity assumption.

In the visible wavelengths, where atmospheric scattering and absorption can be neglected, the reflectivity, and fraction of energy transmitted through clouds, is strongly dependent on the optical depth and the solar zenith angle (SZA). For conservative multiple scattering and reflections within the clouds [Coakley and Chylek, 1975; K99] the cloud reflectivity can be approximated by $R_V \sim 1 - 2\mu_0/(\tau_C^* + 2\mu_0)$, where τ_C^* is defined in terms of the cloud optical depth τ_C , $\tau_C^* = (1 - g)\tau_C$ with $g = 0.848$ for Cl-cloud model [Deirmendjian, 1969] and $\mu_0 = \cos(\text{SZA})$. In the UV, multiple scattering between the clouds and the atmosphere greatly reduces the SZA θ dependence. For UV wavelengths that are not strongly absorbed by ozone, $dR_V/d\theta$ is of the order of 10^{-3} – 10^{-4} per degree ($\sim 6.7 \times 10^{-4}$ for $\lambda = 310$ nm). In the UV, where the ground reflectivity is small (no snow or ice) and can be neglected relative to cloud reflectivities, the scene reflectivity can be approximated by R_V and associated with cloud optical depth for a given cloud fraction. The increased UV reflectivity at high latitudes is directly associated with increasing cloud amounts (optical depth and/or cloud fraction).

The relationship between reflectivity and cloud amount is not so direct in the visible wavelengths, even though atmospheric scattering and absorption are small, since the visible reflectivity R_V is a strong function of the SZA and depends on a variable (seasonally and geographically) ground reflectivity over land.

2. Long-Term Precision of TOMS Reflectivity

The key parameter in estimating LER changes is the long-term precision (stability) of the Nimbus-7/TOMS radiance data measured at 340, 360, and 380 nm. Analysis of the in-flight calibration of TOMS indicates a measured radiance accuracy of $\pm 3\%$ and a precision of better than $\pm 1\%$ per decade. The derived reflectivities have an accuracy of ± 0.5 RU in absolute reflectivity units; that is, if the scene reflectivity is determined to be 10 RU, the result is that the LER is between 9.5 and 10.5 RU. The precision value is ~ 3 times better than the accuracy or about ± 0.2 RU. LER values estimated from the more recent Earth-Probe/TOMS should be more accurate, since both components of the I/F ratio (measured Earth radiance to measured solar irradiance ratio) are determined from TOMS using an improved three-diffuser plate assembly for observing the sun instead of the Nimbus-TOMS single diffuser plate. Use of I/F cancels most of the uncertainties in the radiometric calibration of the spectrometer and the diffuser plate reflectivity. Because of the break in data between Nimbus-7/TOMS and Earth probe/TOMS (break from May 1993 to August 1996), the extended time series cannot be used to estimate trends with the required accuracy until Earth probe/TOMS has operated for a few more years and corrections are applied for any instrument calibration differences.

A demonstration of the stability of R_{380} and the TOMS 380

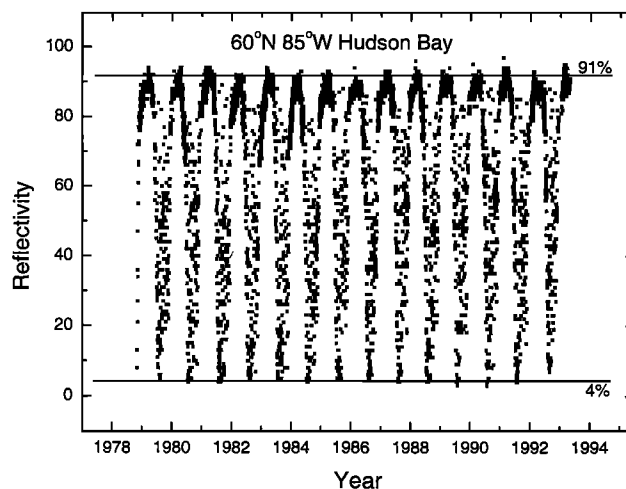


Figure 1. Reflectivity time series over Hudson Bay Canada at 60°N, 85°W. The data are from November 1978 to May 1993.

nm radiance channel is shown in Figure 1, using the reflectivity time series for Hudson Bay (60°N 85°W). As shown, there is a winter ice/snow/cloud reflectivity of $91 \pm 2\%$ (without outliers) and a clear-sky freshwater reflectivity of $4 \pm 1\%$. From the maximum and minimum R values there is no sensible drift of the TOMS instrument, except for a small change near the end of 1992 to May 1993, where it appears that the minimum reflectivity may be biased about 2% high. Part of this bias may be associated with the heavy aerosol loading from the Mount Pinatubo eruption in June 1991, from the satellite orbit drift (from near noon to about 1045) which occurred during the last years of operation of Nimbus 7/TOMS, or from increasing problems with the on-orbit calibration during 1993.

The reflectivity characteristics of Hudson Bay are more useful than those of Greenland, which has an annual mean of 94.5%, and almost no days with $R < 86\%$ because of the continually present ice/snow cover. Hudson Bay has the advantages that every year the snow and ice are fresh, the surface is essentially flat with a minimum of shadows, and during the summer months, the water is very clean with repeatable reflectivity. Greenland has seasonally changing snow/ice characteristics and shadows from hills that can change the effective scene reflectivity. The Hudson Bay values of 91% reflectivity for clouds plus snow/ice and 4% for clean water in the absence of clouds are similar to other snow-covered or open ocean areas of the Earth.

For Nimbus 7/TOMS, values of the extraterrestrial irradiance are obtained from a single ATLAS-3 SUSIM spectrum [Woods *et al.*, 1996] and applied to the entire data record on the assumption that the solar irradiance spectrum is time invariant [Lean, 1997] for 300–400 nm aside from a Sun-Earth distance correction. The TOMS measured solar irradiances at its six wavelengths are normalized to the SUSIM measured extraterrestrial irradiances at the beginning of the TOMS data record (November 1978). The accuracy of the measured ATLAS-3 SUSIM extraterrestrial irradiance is estimated to be $\pm 3\%$.

3. Reflectivity Time Series

Zonal-average reflectivity time series are shown in Figure 2 expressed in percent, while in all subsequent figures, reflectivities are expressed in reflectivity units RU (10% reflectivity =

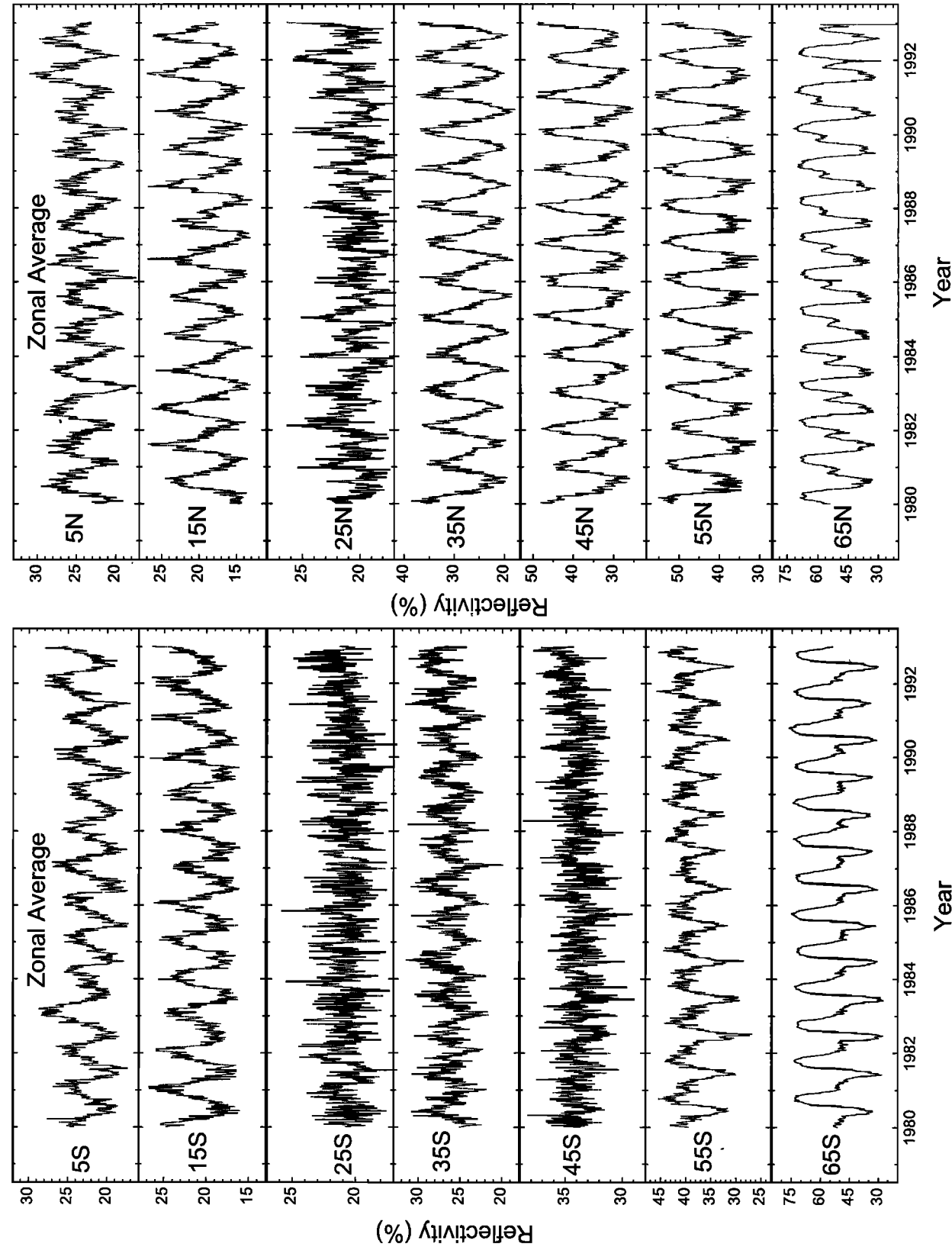


Figure 2. Zonal averages of the weekly average 380 nm reflectivity. (left panel) Southern Hemisphere; (right panel) Northern Hemisphere.

10 RU). This is done to avoid semantic confusion in units with percentage errors and percentage change in reflectivities. The TOMS-measured reflectivity varies rapidly from day to day between 2 RU (clear skies over vegetation), 4 RU (clear skies over bare ground), and 4–8 RU (clear skies over ocean) to 10–50 RU (cloudy scenes and clear skies over snow), and to nearly 100 RU (clouds over fresh snow) [Herman and Celarier, 1997; Herman *et al.*, 1999, H2000]. At middle and high northern latitudes (greater than 35°, see Figure 2), the TOMS-measured reflectivity has a maximum in the winter averaged over both land and water and a minimum during the summer, including the changing amount of snow/ice cover in the winter season. In the equatorial region the reflectivity is a maximum in June–July (0° to 20°N) or in December–January (0° to 20°S). The equatorial differences are caused by the motions of the Intertropical Convergence Zone (ITCZ) band of clouds, located north of the equator during April to August and south of the equator during October to February. Because of the effect of land distribution on tropospheric winds, the ITCZ clouds move to higher latitudes in the Northern Hemisphere than in the Southern Hemisphere, producing a small interhemispheric asymmetry between $\pm 20^\circ$.

In both hemispheres there is a transition band between 20° and 30° where the seasonal dependence changes from the equatorial pattern to that for the middle latitudes (maximum in winter and minimum in summer). The transition bands have extremely high short-term variability relative to other latitude bands.

In the Southern Hemisphere there is another transition-type band at 40°–50°S (crossing southern Argentina and Chile) which shows high short-term variability and little clear seasonal dependence. Poleward of this band (50°–70°S), the pattern shifts again to where there is a maximum during summer (December–January) and a minimum during winter (June–July). The high-latitude reflectivity differences between the Northern and the Southern Hemispheres (NH and SH) are caused by the differences in the relative amounts of land and ocean. In the 40° to 60° band the North contains mostly land and the South mostly ocean. The high reflectivities in the NH are caused by snow/ice and clouds in the winter, while the high reflectivities in the SH are caused by the increased cloudiness from the formation of summer stratocumulus over the oceans.

The seasonal and day-to-day variability is caused by the amount of cloudiness in each zonal band. Monthly-average reflectivity values approximately follow the patterns shown in the maps of UV irradiance [Herman *et al.*, 1999], with high reflectivity corresponding to regions of low UV irradiance. These patterns are substantially the same from year to year. Of interest in this study is the long-term change in reflectivity relative to the annual zonal average, the long-term changes as a function of latitude and longitude, and also when solar cycle and ENSO effects are taken into account.

The zonally averaged annual reflectivity increases from about 20 RU at 30°, to over 50 RU near 70°, and to 80 RU over the polar ice caps in both hemispheres (see Figure 3). In the range from 30°S to 30°N the annual average reflectivity is about 20–25 RU. Annual average reflectivity values are slightly larger in the Northern Hemisphere than in the Southern Hemisphere. Since the surface reflectivity in the UV is about 2–8 RU over land and oceans, the additional reflectivity is mostly due to cloud cover with a small addition (about 5 RU) for aerosols. In terms of exposure to UV irradiance at the Earth's surface, the cloud cover produces an average fractional

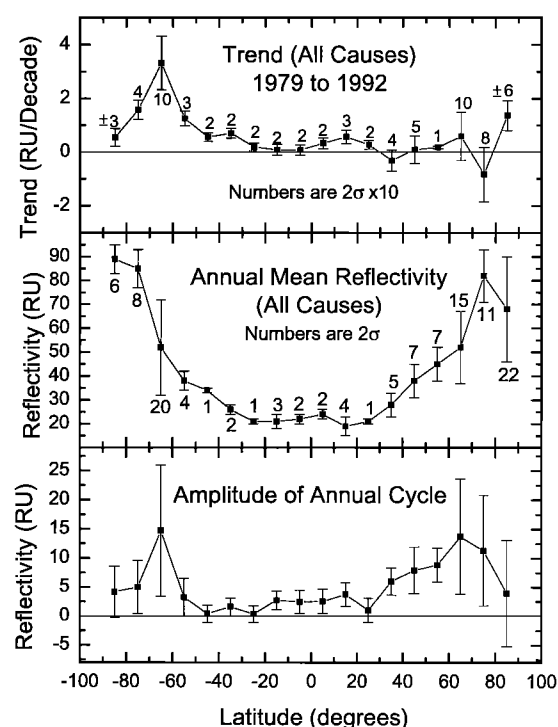


Figure 3. (a, top) Linear-fit trend per decade (b, middle) annual mean 380 nm reflectivity, and (c, bottom) amplitude of annual 380 nm reflectivity cycle between $\pm 90^\circ$ from all causes for the period 1979 to 1992. All error bars are 2 standard deviations (2σ).

reduction of the order of $1 - R$ during the summer (e.g., 0.2–0.3 for midlatitudes), relative to clear-sky values [Ziemke *et al.*, 1998; Herman *et al.*, 1999; K2000].

It is important to note that the TOMS estimates of scene reflectivity apply only to the ~ 1100 to noon local solar time of the Nimbus-7/TOMS overpass of each point on the Earth's surface. Because of this, any long-term changes in early morning or late afternoon scene reflectivities are not observed by TOMS. Over the life of Nimbus 7/TOMS, November 1978 to May 1993, the orbit overpass time shifted between local noon and 1045. Long-term well-calibrated observations from space of the entire sunlit Earth would be necessary to determine the diurnal variation of reflectivity (e.g., from geostationary or Lagrange-1 orbits).

4. Zonal Mean, Annual Amplitude, and Long-Term Change

The results of directly taking zonal averages of the reflectivity data in 10° latitude bands (see Figure 2) and calculating the slope from a linear fitting of the 18 time series from -90° to 90° are shown in Figure 3a. Figures 3b and 3c show the annual mean reflectivity as a function of latitude and the amplitude of the annual cycle. These results include all causes contributing to the reflectivity and reflectivity changes.

The Northern Hemisphere shows smaller zonal-average changes in reflectivity at middle and high latitudes than the Southern Hemisphere. The error bars represent the 2 standard deviations (2σ) in the reflectivity and reflectivity change from all causes. In general, this method overestimates the error bars for both the reflectivity and the long-term reflectivity changes

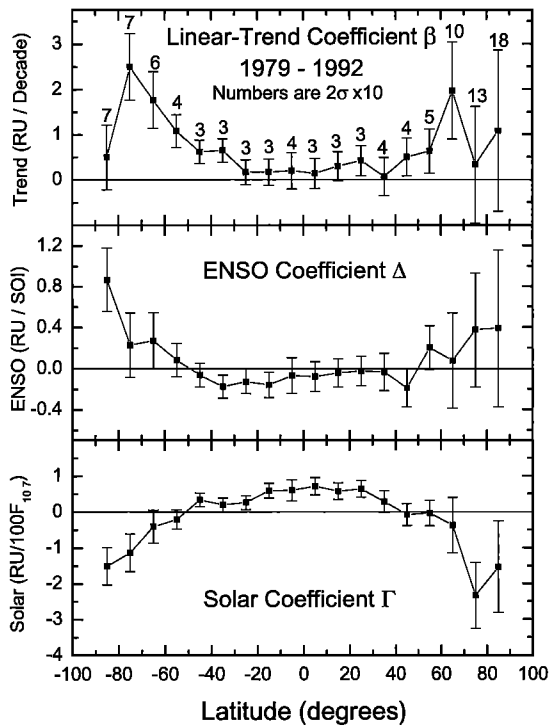


Figure 4. (a, top) Linear-trend coefficient β (compare Figure 3a), (b, middle) ENSO coefficient Δ , and (c, bottom) the solar coefficient γ in equation (3) in units of RU per year, RU per SOI, and RU per 100 $F_{10.7}$, respectively. Error bars are 2σ standard deviations. The small numbers on the error bars in Figure 3a are $2\sigma \times 10$. SOI is the Southern Oscillation Index.

by including cyclic effects. After removal of these effects, the interhemispheric differences in reflectivity are significant. The estimated reflectivity changes shown in Figure 3a are consistent with previous statistically nonsignificant estimates of zonal-average UV reflectivity changes between $\pm 55^\circ$ latitude [Herman et al., 1996].

The remainder of this paper discusses the estimation of near-noon LER changes (1980–1992) as a function of latitude and longitude in terms of a time series analysis, including the effects of annual cycles, solar cycle, and ENSO effects. The results are applied to an estimation of the increased amount of radiation reflected back to space. The basic data used are the reflectivities estimated from Version-7 Nimbus-7/TOMS-measured 380 nm radiances over the latitude range from 82°S to 82°N , including regions permanently covered with ice or snow.

5. Least Squares Time Series Analysis

A 14-year time series can be formed from the LER reflectivities determined for each of the pixels from a $1^\circ \times 1^\circ$ (latitude \times longitude) daily gridded data set. There are several distinct types of reflectivity time series depending on whether the scene is located in a coastal or mountain area (strong annual cycle), in an inland plain area (large day-to-day variance but little annual cycle), or an area with seasonal snow cover (strong annual or semiannual cycle). In addition to these seasonal and annual patterns, there are clear correlations with ENSO and 11.3-year solar cycle effects.

In this study we applied a linear regression model R_{FIT} to

each grid-point time series to help identify the different mechanisms likely to be responsible for monthly to decadal variations in 1980–1992 Nimbus-7 TOMS 380 nm reflectivity R measurements [similar to Stolarski et al., 1991; Ziemke et al., 1997 for ozone changes]:

$$R_{\text{FIT}} = \alpha(t) + \beta t + \gamma S_{\text{SOLAR}}(t) + \Delta E_{\text{ENSO}}(t) + \varepsilon(t). \quad (3)$$

Here t represents a time index, and $\alpha(t)$ is a time-dependent regression coefficient given by a constant plus 12-, 6-, and 4-month cosine and sine harmonic series. Quantities β (RU/year), γ (RU/100 $F_{10.7}$), and Δ (RU/SOI) were taken to be constants, and $\varepsilon(t)$ represents the residual-error time series of the model. $S_{\text{SOLAR}}(t)$ is the solar proxy ($F_{10.7\text{-cm}}$ solar-flux series was used), and $E_{\text{ENSO}}(t)$ is given by the Tahiti minus Darwin sea level pressure time series (e.g., the Southern Oscillation Index (SOI)). The coefficients are determined by a least squares fitting of $R_{\text{FIT}}(t)$ to $R(t)$ and are shown in Figure 4.

6. Annual Zonally Averaged Reflectivity Changes

Each day's reflectivity estimates are averaged together in 10° latitude bands centered on $[-85^\circ, -75^\circ, -65^\circ, \dots, 85^\circ]$ to form time series from 1980 to 1992. These 18 time series are approximated by least squares fitting using (2) with the coefficients plotted in Figure 4. Error bars are indicated at each latitude-band point representing 2 standard deviation uncertainties. As shown in Figure 4, there are statistically significant ENSO effects in the reflectivity time series at southern mid-latitudes from 10°S to 40°S , and solar-cycle effects from 50°S to 40°N . Both of these are small effects (about 1 to 3 RU).

The linear-trend coefficient β (see Figure 4a) is different than the trend due to all causes (see Figure 3a). Most notable is the shift in the maximum value from 65°S to 75°S when solar cycle and ENSO effects are removed, the appearance of statistically significant trends in the Northern Hemisphere high latitudes, and small statistically significant trends at midlatitudes. The linear-fit trend becomes significant poleward of 40°N and 30°S , with no significant changes occurring in the equatorial and lower middle latitudes. The Northern Hemisphere trends were masked mostly by the solar-cycle effect.

Before removal of the solar-cycle effect from the linear-fit trend, there appeared to be a small statistically significant change in reflectivity near the equator (0.3 to 0.5 ± 0.2 RU per decade) and less of a trend at higher latitudes. Reflectivity changes are larger in the Southern Hemisphere (0.5 to 1.0 ± 0.2 RU per decade at latitudes that include land and about 1.8 ± 0.2 RU per decade over the ocean). There are large changes in reflectivity in regions over or near ice sheets in both hemispheres. The largest reflectivity change is in the latitude range between 60°S and 70°S and amounts to about 3.3 ± 1 RU per decade (see Figure 4).

From Figure 4 the changes over the Antarctic continent are much smaller (zonal average change of 0.5 to 1.5 ± 0.3 RU/decade) than those over adjacent regions of ocean. Note that the Antarctic observations are representative of only mid-September to mid-March and the Arctic from mid-March to mid-September when the areas are illuminated by the direct Sun.

From TOMS data alone there is no way to distinguish between changes in reflectivity caused by clouds or snow/ice.

However, there is evidence from satellite microwave observations that the amount of sea ice in Antarctica has increased in area and extent at a rate of about $1.4000 \pm 0.2500 \times 10^4 \text{ km}^2$ per year for the period 1978 to 1996 [Cavalieri *et al.*, 1997], which would contribute to the observed reflectivity increase. For the Arctic there has been a decrease of $3.1 \pm 0.5 \times 10^4 \text{ km}^2$ per year. Expressed in percent, these are $1.3 \pm 0.2\%$ for the Antarctic and $-2.9 \pm 0.4\%$ for the Arctic per decade. However, for the period 1978 to 1993 the amount of Antarctic ice showed no significant trend. Data obtained after 1996 (D. J. Cavalieri, private communication, 2000) tend to reduce the rate of increase of sea ice. The near-null result for 1978 to 1993 implies that the decadal changes seen by TOMS in the Antarctic were largely changes in cloud reflectivity. In the Arctic there is no statistically significant change in reflectivity from all causes (see Figure 3 in contrast to Figure 4), which corresponds to the decrease in sea-ice amount.

The scene reflectivity (clouds, aerosols, and surface) varies considerably within a latitude band, depending on whether the area considered is over land or water. There are clear patterns in the cloud reflectivity related to ocean currents, major wind systems, mountain areas, etc. These monthly and annual patterns are largely repeatable from year to year over the entire globe. In the UV, monthly variations in surface reflectivity for both oceans and land are small except when there is seasonal snowfall. The details of this variation are discussed in another paper (H2000).

As shown in Figure 5, the increasing reflectivity with increasing latitude (see Figure 3) is almost perfectly balanced to a uniform effective area-weighted reflectivity of about $21 \pm 3 \text{ RU}$ between $\pm 75^\circ$ latitude. Since the solar energy reflected from the Earth is proportional to the area of the Earth's surface as a function of latitude, it implies that a percentage change in reflectivity at any latitude between $\pm 75^\circ$ is important for the Earth's energy balance.

From the viewpoint of absolute (as opposed to relative) reflectivity change, changes at low latitudes, 0° – 25°N and 25°S , are most important because of the relatively low noontime solar-zenith angles (less than 40°) compared to other regions. Within the equatorial zone (23°S – 23°N) the solar zenith angle conditions are always equivalent to middle-latitude summer.

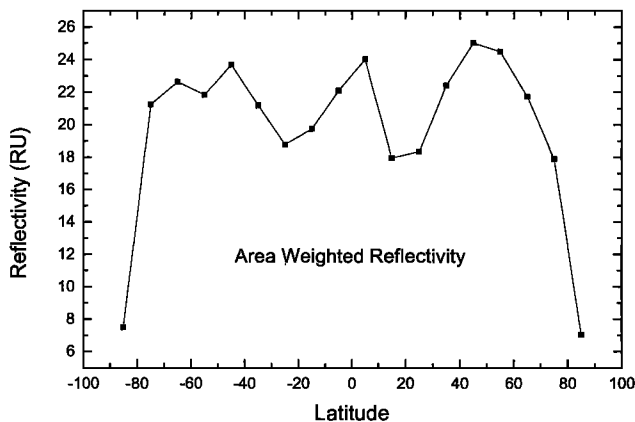


Figure 5. Annual area-weighted zonal-average reflectivity, $R \cos(\text{lat})$. The two dips in reflectivity near 20°N and 20°S are related to the sinking air from presence of the Hadley-cell structure.

Table 1. Solar Power Spectrum Above the Earth's Atmosphere

$\lambda_{\text{Min}}, \text{nm}$	$\lambda_{\text{Max}}, \text{nm}$	Power, W/m^2	Percent of 1370, W/m^2
0	300	16	1.2
300	1000	935	68.2
1000	2000	337	24.6
2000	4000	70	5.1
4000	15000	12	0.88
15000	∞	0.23	0.02

7. Power Reflected to Space

The change in solar energy reflected back to space can be estimated from changes in the TOMS 380 nm zonal-average reflectivity. The following assumptions are used: (1) The rate of change in reflectivity at 380 nm is the same for all wavelengths containing most of the incident solar energy (see Table 1). (2) The reflectivity change mostly represents the change in cloud reflectivity plus change in ice/snow reflectivity with only small contributions from ground or water reflectivity. This is because the 380 nm reflectivity of the ground or water is always less than 8% and most often is 2–4%. (3) Rayleigh scattering is not included in the calculation because it does not change significantly from year to year, and it is not significant in the visible wavelengths where most of the incident solar energy is contained. (4) Atmospheric absorption (e.g., by ozone, water vapor, aerosols) is neglected. (5) The incident solar irradiance on the Earth is proportional to $I_0 \cos(\theta)/a^2$ and the reflected radiation proportional to both the zonal area and the scene reflectivity $R_S \cos(\phi)$, where I_0 is the solar irradiance at the top of the atmosphere, $\theta = \text{SZA}$, $a =$ the Sun-Earth distance in AU, and ϕ is the latitude. (6) The long-term changes in monthly averaged zonal-average TOMS reflectivity are representative of the long-term changes in the reflectivity over the entire sunlit Earth. This assumption is helped by the effect of increased solar zenith angles for times away from noon.

The incident solar energy on the Earth is about 1370 W/m^2 based on the Nimbus-7/ERBE and SMM/ACRIM measurements [Willson, 1993]. Of this, about 30% is reflected back to space (411 W/m^2), 50% is absorbed at the surface, and 20% is absorbed in the atmosphere [Harrison *et al.*, 1993]. Other energy partitioning is given by Ramanathan and Volgelmann [1997] (30%, 42%, and 28%, respectively). As a function of wavelength λ , the energy is distributed as shown in Table 1, with most of the incident solar energy between 300 and 4000 nm.

If we assume that the reflectivity of the Earth's atmosphere and surface can be represented by an equivalent zonal-average Lambertian reflectivity $R = R(\phi, t, \delta)$, the total power per Earth cross-sectional area (πR_{EARTH}^2) reflected from the sunlit Earth in the latitude band $d\phi$ is

$$dP(\phi, t) = d[I_0 \langle R \rangle] \\ = \frac{I_0}{\pi a^2} d\phi R(\phi, t) \int_{S_R}^{S_S} dL \cos(\theta) \cos(\phi), \quad (4)$$

where ϕ is the latitude, L is the longitude, θ is the solar zenith angle, δ is the solar declination angle, a is the Sun-Earth distance (in AU), t is time, and the sunrise S_R and sunset S_S longitudes are

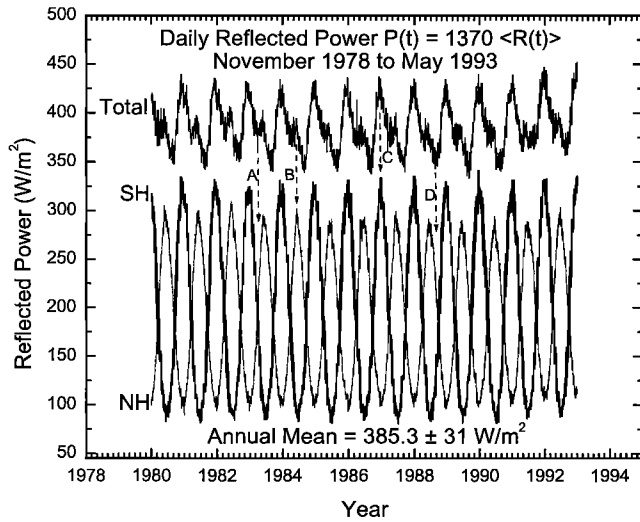


Figure 6. Daily reflected-power time series based on equations (4)–(7) with $I_0 = 1370 \text{ W/m}^2$. The 14-year annual mean is $385.3 \pm 31 \text{ W/m}^2$ based on UV-reflectivity data. Contributions to the global reflected power from the NH and SH are shown. The SH summer dominates the NH summer because of the difference in Sun–Earth distance. SH (thicker line) NH (thinner line). The arrows A and B mark the secondary maxima and minima, and D and E mark the annual maxima and minima.

$$\begin{aligned} S_R &= -\cos^{-1}(-\tan \phi \cdot \tan \delta) & \sin S_R &= -[1 - \tan^2 \phi \tan^2 \delta]^{1/2}, \\ S_S &= +\cos^{-1}(-\tan \phi \cdot \tan \delta) & \sin S_S &= +[1 - \tan^2 \phi \tan^2 \delta]^{1/2}. \end{aligned} \quad (5)$$

The solar zenith angle can be expressed as

$$\cos(\theta) = \cos(\phi) \cos(\delta) \cos(L) + \sin(\phi) \sin(\delta). \quad (6)$$

Substituting (5) and (6) into (4) yields the following three cases: case 1, no illumination in winter polar region.

NH $\delta < 0$ and $\phi > \pi/2 + \delta$

for December solstice: $\phi > 66.55^\circ$.

SH $\delta > 0$ and $\phi < -\pi/2 + \delta$

for June solstice: $\phi < -66.55^\circ$.

Case 2, middle and equatorial latitudes in both hemispheres:

$$-\pi/2 + \delta \leq \phi \leq \pi/2 - \delta \quad \text{at solstice: } |\phi| \leq 66.55^\circ.$$

$$\begin{aligned} dP(\phi, t) &= \frac{2I_0}{a^2\pi} d\phi R(\phi, t) \\ &\cdot [S_S \cos \phi \sin \phi \sin \delta + \sin S_S \cos^2 \phi \cos \delta]. \end{aligned} \quad (7)$$

Case 3, $|\phi| > \pi/2 - |\delta|$ in summer polar regions. At solstice $|\phi| > 66.55^\circ$.

$$dP(\phi, t) = \frac{2I_0}{a^2\pi} d\phi R(\phi, t) [\cos \phi \sin \phi \sin \delta] \quad (8)$$

In the special case of $R_m(\phi) = R = \text{constant}$ and $\delta = 0$, the integral of (7) over the range $-\pi/2 \leq \phi \leq \pi/2$ gives $P = I_0 R/a^2$, as expected.

For the remainder of this section the diurnal variation of the Earth's atmosphere is neglected, with all longitudes having zonally averaged near-noon values of physical quantities (e.g., reflectivity $R(\phi, t, \delta)$) as measured by TOMS.

The global quantity $\langle R \rangle$ can be obtained from (4) to (8) with $\phi_1 = -\pi/2$ and $\phi_2 = +\pi/2$, using the TOMS zonally averaged monthly 380 nm reflectivity time series. The results are illustrated in Figure 6. The change in reflected power caused by changes in reflectivity is

$$\Delta P_r = I_0 \langle \Delta R \rangle = 2.8 \pm 2.8 \text{ W/m}^2 \text{ per decade}, \quad (9)$$

with $\langle \Delta R \rangle = 0.0073$ per decade, where $\langle \Delta R \rangle$ is the trend in $\langle R(t) \rangle$ in (4) (see Figure 6) with $I_0 = 1370 \text{ W/m}^2$. The trend numbers are based on time series analysis, as in (3), and the error estimates are 2 standard deviations. The 14-year annual average reflected power based on UV reflectivity is $385.3 \pm 31 \text{ W/m}^2$ (see Figure 6). This amount is less than the previously estimated values of 411 W/m^2 [Harrison *et al.*, 1993]. Part of the reason for the difference is that the UV reflectivity underestimates higher reflectivity of the Earth's surface (ground and ocean) for visible wavelengths. Both ΔP_r and P_r would be reduced by 3% (to 2.7 and 372) if the incident energy between zero–300 nm and 4000 to ∞ is not included.

The seasonal and latitudinal details for $P_r = I_0 \langle R \rangle$ during a typical year are shown in Figures 6, 7a, and 7b, based on incident solar power of $I_0 = 1370 \text{ W/m}^2$. The maximum power reflected back to space occurs during the months from November to February (maximum in January (Figure 7c)), and the minimum is during July (Figure 7d) (see arrows in Figure 6, also Figure 7b). The ratio between the global annual minimum and the maximum reflected power is $\delta P_r = 22\%$. The difference between the NH and the SH summer maxima is about 5.8% and is mostly caused by the difference in summertime Sun–Earth distance between January and June. For incident power I_0 , the difference in Sun–Earth distance accounts for $\delta I_0 = 6.7\%$. The May secondary peak B in the total reflected power is from the May maximum in the NH. The July annual minima D in the total reflected power occurs shortly before the contribution from the NH and SH are equal (September and March) with the secondary minima A in March.

The largest contribution to P_r comes from the equatorial latitudes (see Figure 7a), with substantial amounts from mid-latitudes ($\pm 50^\circ$). Because of the approximate $\cos^2 \phi$ weighting (from $\cos \theta \cos \phi$), the main regions contributing to the reflected power have a broad latitude dependence centered on the equator somewhat similar to the area-weighted reflectivity shown in Figure 5.

During November to February the NH has a partial cover of snow/ice over a considerable latitude range (40° – 90°) as well as increased seasonal cloudiness. Increased reflectivity for either of these contribute to increased reflected power to space. There is a winter hemispheric asymmetry because the land distribution in the SH is toward lower latitudes compared to the NH, causing a much smaller winter-snow/ice increase in reflectivity. The SH is mostly water covered from 40° to 65° . The April to September SH cloudiness over water is not so reflective as the October to March NH cloudiness over snow/ice. Large regions of clouds over water tend to be about 40 RU, except for comparatively small regions over storms or stratocumulus clouds. The reflectivities of clouds over snow/ice fre-

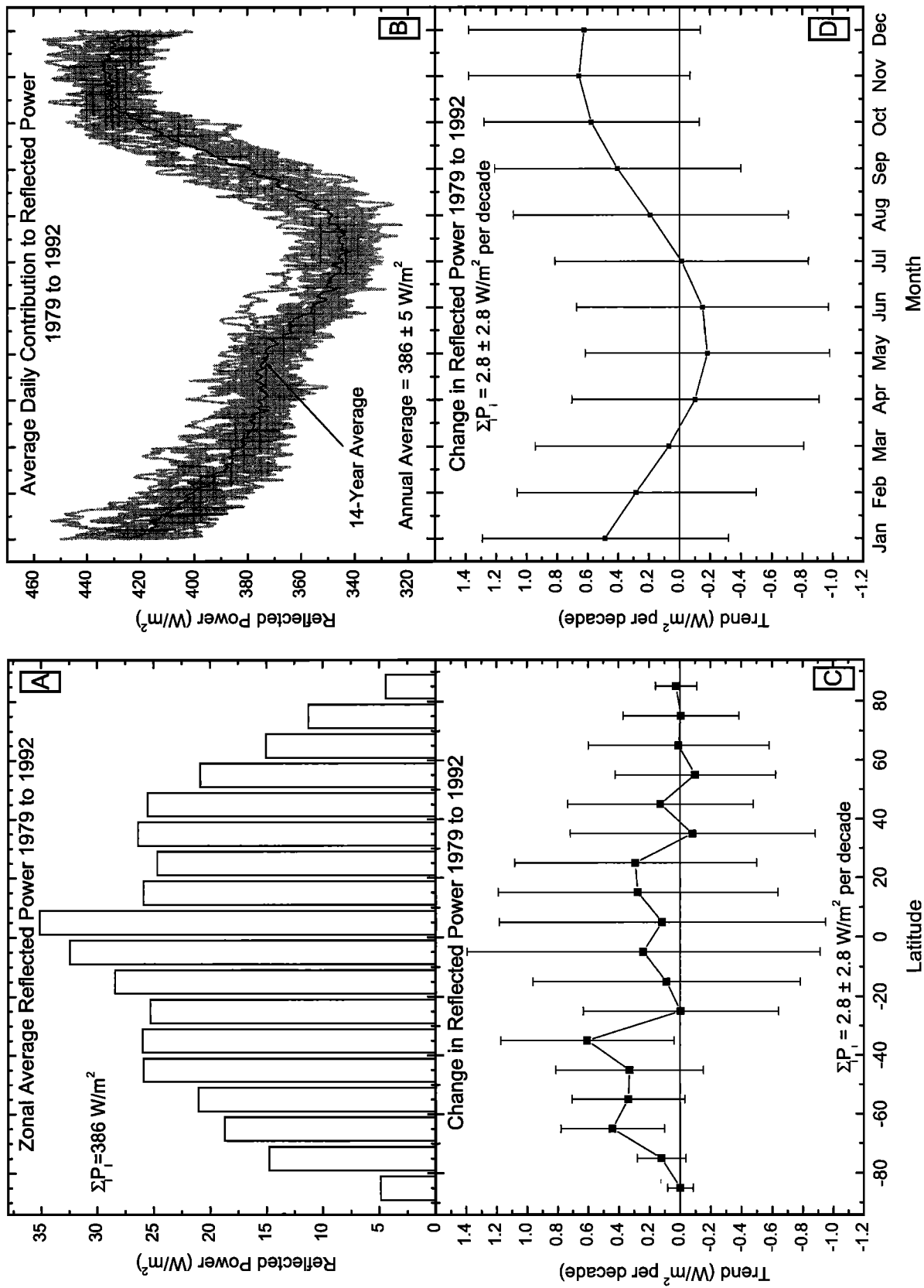


Figure 7. (a) Contribution to reflected power $I_0\langle R \rangle$ by latitude with $I_0 = 1370 \text{ W/m}^2$. (b) Fourteen-year average daily contribution to reflected power $I_0\langle r \rangle$ with $I_0 = 1370 \text{ W/m}^2$. The gray area represents the reflected power for the 14 annual time series. (c) Reflected-power trend $\Delta P_i = \Delta(I_0\langle R \rangle)_i$ by latitude. (d) Reflected-power trend $\Delta P_i = \Delta(I_0\langle R \rangle)_i$ by month. All error bars are 2σ .

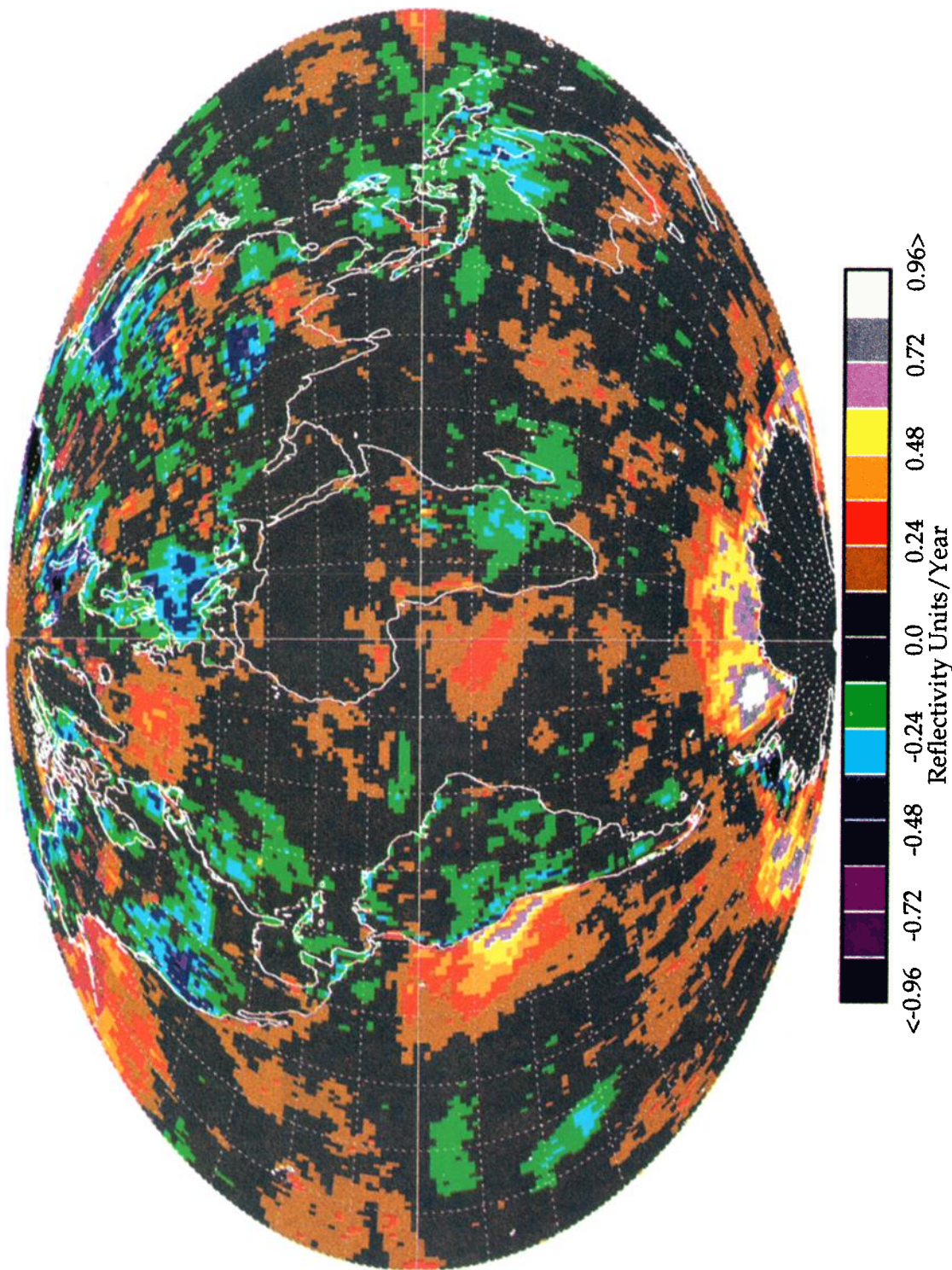


Plate 1. Contour plot of the linear slope coefficient (RU per year) for all causes (see Figure 3) showing a map of the global trends in annually averaged reflectivity for 1980–1992 for each $1^\circ \times 1^\circ$ TOMS pixel from the gridded reflectivity data set. The same features and changes are obtained when the pixels are averaged into $5^\circ \times 5^\circ$ boxes (25 pixels per box), or when 50-day low-pass Fourier smoothing is applied.

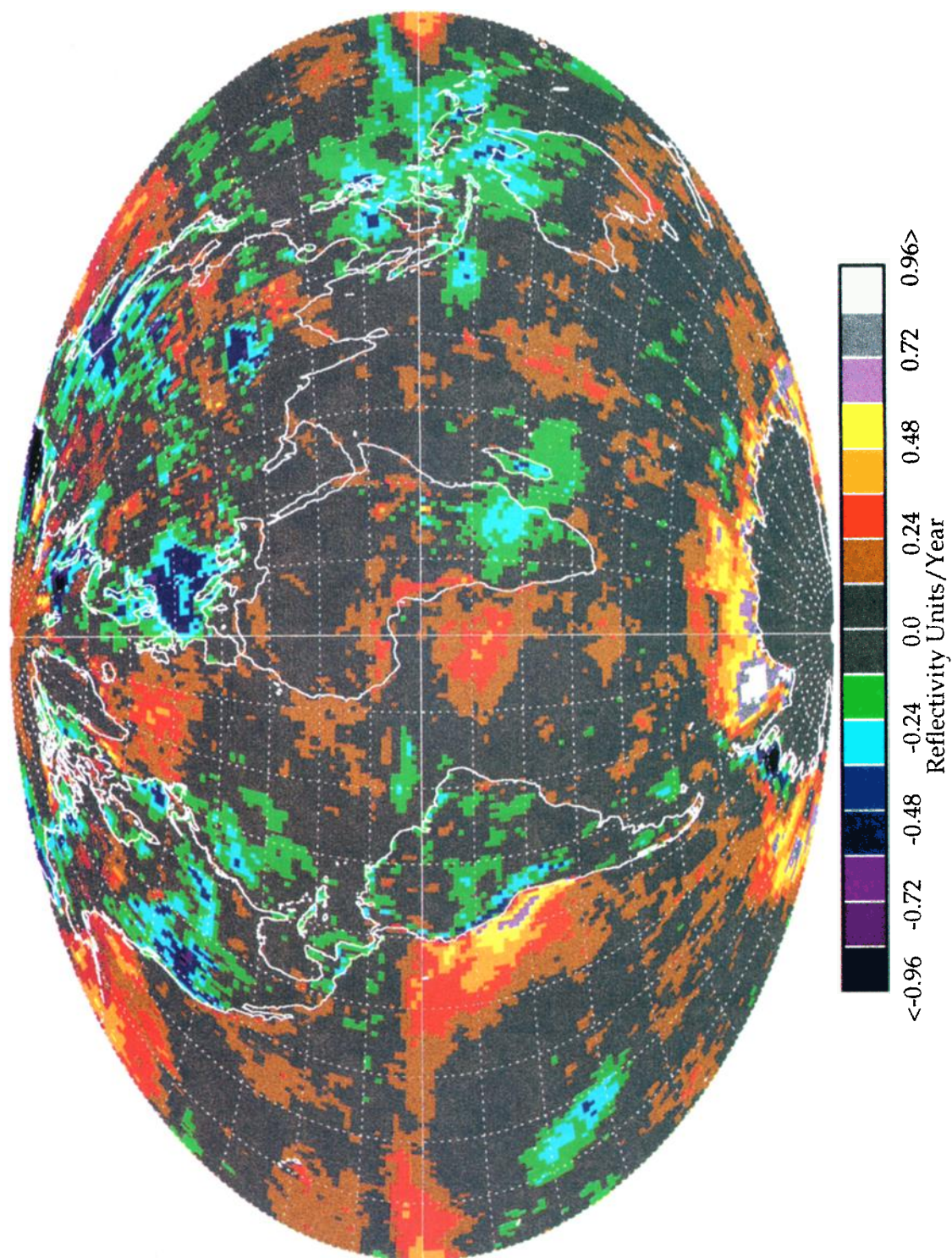


Plate 2. Similar to Plate 1 but estimated from equation (3) with the solar and ENSO effects removed. Fifty-day low-pass Fourier transform smoothing was applied to the data prior to estimation of the trends.

REFLECTIVITY TREND FOR 1980 THROUGH 1992

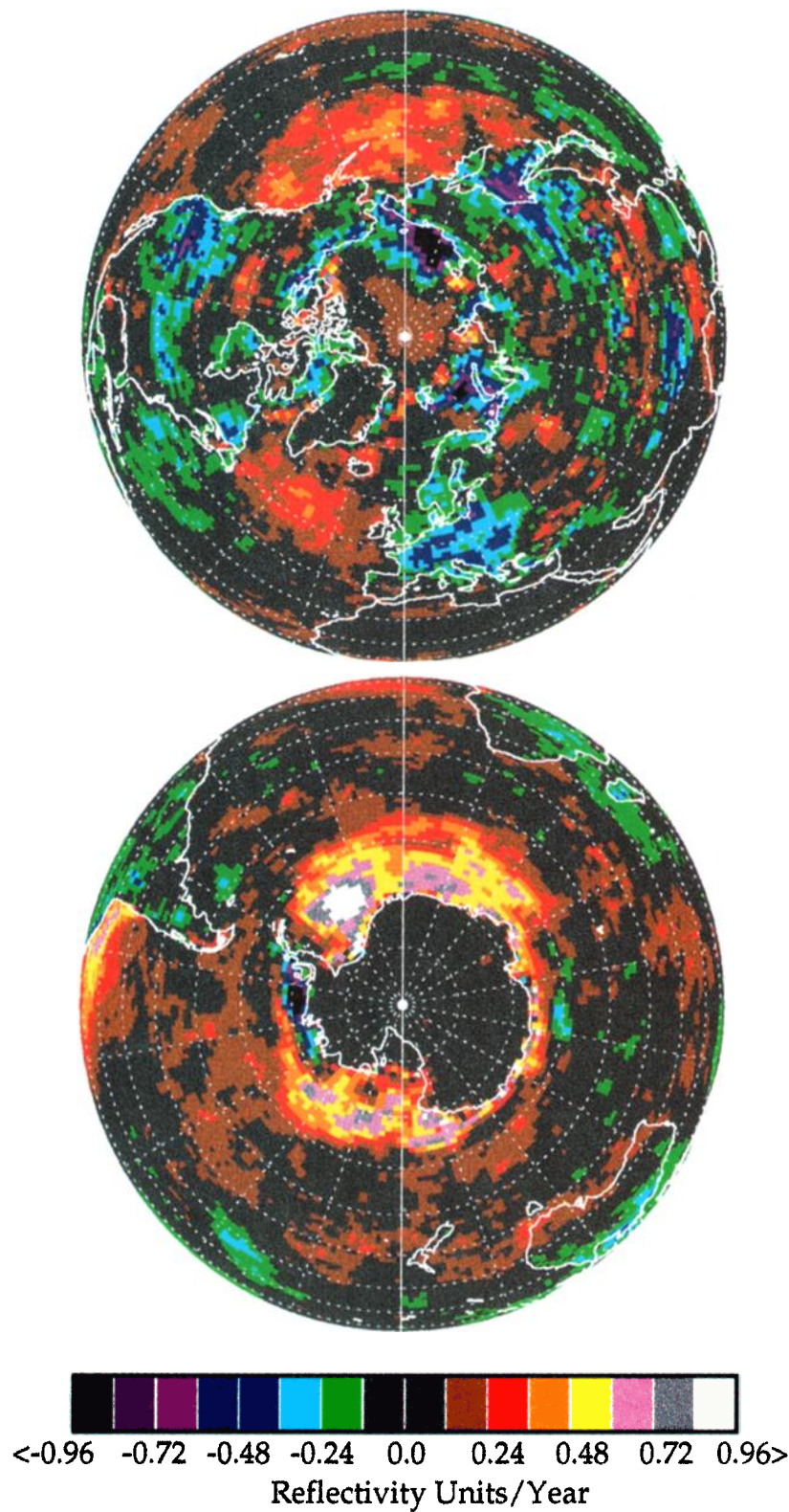


Plate 3. Polar views of the trend data contained in Plate 2 with the Arctic in the top half and Antarctic in the bottom half.

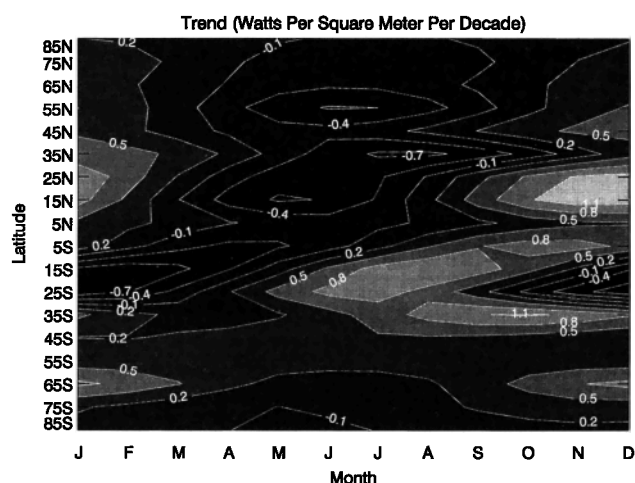


Figure 8. Zonally averaged solar power reflected back to space as a function of latitude and month. The light areas make the largest contribution to the global increase in reflected power.

quently are 80–92 RU with the underlying snow/ice having a reflectivity of 20–90 RU depending on the terrain, depth of snow, and the age of the snow.

Figures 7c and 8 show the contribution ΔP_i of each latitude band to the decadal trend in reflected power $\Delta(I_0 \langle R \rangle)$. When examined by month (see Figures 7d and 8), the largest contribution to $\Delta(I_0 \langle R \rangle)$ comes from the November to January months. Because of the weighting by solar zenith angle and latitude, $\Delta(I_0 \langle R \rangle)$ does not follow the largest changes in reflectivity, as shown in the next section (see Figure 9).

From Figure 8 the largest changes in ΔP come from November to January at equatorial latitudes (20°S–20°N) and from the Southern Hemisphere midlatitudes (15°S–45°S) during the winter and spring months. The $\sim \cos^2 \phi$ weighting effectively removes the global effects of the larger reflectivity changes at high latitudes on the reflected power, even though important locally for changes in reflected power and radiation reaching the Earth's surface.

8. Changes by Month and Latitude

Figures 3 and 4 show that there have been statistically significant increases in the annual zonally averaged cloud reflectivity, mostly at middle and high latitudes. Because of the large seasonal effect in the amount of solar radiation striking the Earth at different latitudes (i.e., winter versus summer), it is important to examine when the changes occur and at which latitudes.

The two-panel Figure 9 shows the zonally averaged reflectivity trends by month for the period 1980–1992. Statistically significant RU increases start at about the 2–3% per decade level and show changes mostly in the middle and high latitudes during the autumn and winter months in both hemispheres. There are some increases at all latitudes with the largest zonal-average increases of 9% per decade occurring at high northern latitudes ($\sim 65^\circ$). While the area (month \times latitude) showing significant reflectivity increases is roughly comparable between the hemispheres, the Northern Hemisphere shows larger increases (+9% per decade maximum in the NH and +5% per decade maximum in the SH). Reflectivity changes during the summer months are small and most are statistically not significant. There are some small regions of reflectivity decreases centered at 15°N during May and 30°N during September. The most important months (summer) for UV radiation at the surface show little change in reflectivity in either hemisphere.

9. Global-Cloud Change Maps

The coefficients β (latitude, longitude), representing the slope of a linear fit to each $1^\circ \times 1^\circ$ grid-point time series of reflectivity R , are plotted in a contour plot (see Plate 1 for all causes) and, using (3), with solar cycle and ENSO effects removed (see Plate 2) to identify regions with the largest increases or decreases between 1980 and 1992.

The linear-fit trends in Plates 1 have been determined in two ways that yield nearly the same results. (1) Linear least squares fitting to the daily reflectivity data (4749 points per time series) and (2) linear least squares fitting to smoothed data using a 50-day low-pass Fourier transform filter (4749 points). After smoothing, the data can be sampled in 30-day intervals without altering the results. Different results were obtained when the

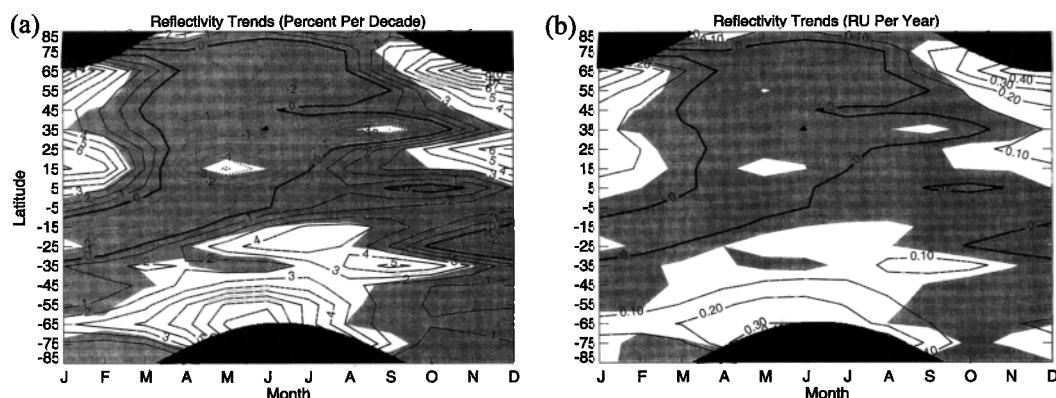


Figure 9. Zonally averaged reflectivity linear trend by month for 1980–1992 with solar and ENSO effects removed. (left) Percent change of RU per decade. (right) Change in RU per decade. Statistically significant changes are shown in regions with a white background. Blackened areas are not sunlit during the months shown.

reflectivity data were averaged over 30 days (leaving 156 data points in the time series) without smoothing. The smaller, monthly-average time series showed large adjacent pixel-to-pixel variations in the estimated trends over the entire globe instead of the highly organized local structure shown in Plates 1 and 2. The noisy results were caused by high-frequency aliasing errors introduced by the presence of transient clouds and the shortened time series. This is purely a statistical result when estimating trends and is not related to the validity of the daily reflectivity data for use in estimating changes in the average UV irradiance in the TOMS FOV or in the power reflected to space.

Since the same trends were obtained with and without smoothing for reflectivity changes from all causes (see Figure 3 and Plate 1), smoothing and monthly sampling were applied to the data prior to using (3). For the reflectivity data set, the use of smoothing followed by monthly sampling makes the resulting matrices and their inverses implied by (3), easier to handle and less prone to inversion error. The matrices are reduced in dimension from 4749×4749 to 156×156 . As shown in Figures 3 and 4, the 2σ error bars are changed but are not substantially different, between the trend from all causes and the trend computed from (3). Since the same trends were obtained with and without smoothing in Plate 1, and the error estimates with smoothing (Figure 4) and without smoothing (Figure 3) are similar, the main trend features in Plate 2 should not be affected by the smoothing.

For the cases shown in Plates 1 and 2 the regions of largest change are just to the west of Chile and Peru (5 RU to 7 RU per decade), small parts of western Europe (-4 RU per decade), western United States (-4 to -6 RU per decade), southern China (-4 to -6 RU per decade), eastern Russia and Europe (-4 to -6 RU per decade), and small regions of 5 RU per decade over land and oceans.

One of the largest regions of reflectivity increase is near the northern edge of the Antarctic ice shelf near the Palmer Peninsula (see the Appendix for polar view). Here reflectivity increases are up to 10 RU per decade, with most of the changes in the range of 5 to 7 RU per decade (about a 10 to 14% increase per decade relative to the 1980 zonal average). While the causes of increases in reflectivity near the ice shelf cannot be determined from TOMS data alone, microwave data indicate that there has been no change in sea-ice amount from 1978 to 1993 [Cavalieri *et al.*, 1997], so that the changes observed are probably from increases in cloud reflectivity. In addition, there are large regions over open water that also show increases in reflectivity of a magnitude that can only be caused by an increase in cloudiness (cloud fraction or optical depth). The region of large increase in reflectivity is confined to a latitude band between 50° and 80° , with a maximum at about 65° . Within this latitude band, it represents an approximate 6% decrease in annual average radiation reaching the ground at all wavelengths in the UV and visible if there have been no changes in surface albedo. If there are changes in surface albedo, they seem to be confined to the Antarctic coastal regions, since the reflectivity change is essentially zero over the ice shelf and in the interior of the Antarctic continent. In either case, the increase in reflectivity represents additional radiation reflected back to space.

In the Northern Hemisphere there is a much smaller region centered on 85° latitude where there has been a reflectivity increase. While it is not possible to separate the increase with changes in cloudiness or with changes in surface albedo from

TOMS data, microwave data from 1978 to 1993 indicates that sea-ice amount has decreased [Cavalieri *et al.*, 1997; Parkinson *et al.*, 1999], so reflectivity increases occurring over ocean areas can be associated with changes in cloudiness.

When the solar cycle and ENSO effects are removed using (3) (see Plate 2), the larger estimated reflectivity changes appear to be approximately the same as those in Plate 1. An exception to this is in the southern Pacific Ocean west of Chile and Peru and for a small region near the equator (about -2 RU per decade). For most of the globe the statistically significant (i.e., larger) local changes in reflectivity between 1980 and 1992 are only altered a little by these two effects. However, the change is sufficient, so it is significant on a global or zonal average basis. The solar-cycle correlation (see Figure 3 and Plate 2) suggests a relationship between weather and solar activity. High-precision measurements over a longer period of at least two solar cycles (about 23 years) would be needed to establish the Sun-weather relationship.

10. Summary

The time series of Lambert equivalent reflectivities for each $1^\circ \times 1^\circ$ scene observed by TOMS between 1980 and 1992 were analyzed to obtain the mean reflectivity as a function of latitude and longitude and to estimate statistically significant linear changes that have occurred over the period. The stability of the TOMS 380 nm reflectivity channel was demonstrated using data obtained over Hudson Bay, Canada. As discussed previously [Herman *et al.*, 1996], there were no significant changes in annual zonal-average cloudiness from all causes (combined optical depth and cloud fraction) over the 1980–1992 period except at high latitudes. When the 11.3-year solar-cycle and ENSO effects are removed from the time series, the zonally averaged annual linear-fit trends show that there have been increases in reflectivity (cloudiness) poleward of 40°N and 30°S , with some smaller but significant changes occurring in the equatorial and lower middle latitudes. Examination of the time series coefficients show that the solar-cycle term partially compensated for a real long-term change in cloudiness. Removal of the solar-cycle effect causes an increase in linear trend for reflectivity between about $\pm 40^\circ$ and a decrease at higher latitudes. When viewed on a monthly basis, most of the changes occur during the autumn and winter months in both hemispheres. There are also statistically significant winter reflectivity increases at low latitudes in the Northern Hemisphere. The 11.3-year period correlation suggests a relationship between weather and solar activity. High-precision satellite measurements over a longer period of at least two solar cycles (about 23 years) would be needed to establish the Sun-weather relationship.

The power-weighted (area and solar zenith angle) global-average reflectivity time series was obtained in order to estimate the increase in radiation reflected back to space from changes in cloudiness, aerosol amount, and surface reflectivity (mostly snow/ice). Applying the TOMS 380 nm reflectivities for all wavelengths between 300 and 4000 nm, the 14-year annual average power reflected back to space is 385.3 ± 31 W/m². This is close to the 411 W/m² estimated from previous studies [Harrison *et al.*, 1993]. For 1980–1992 the overall long-term effect is for an increase in radiation reflected back to space (2.8 ± 2.8 W/m² per decade) with the largest increases coming during the months from November to February and from the Southern Hemisphere. The size of the 2σ uncertainty

(2.8 W/m²) in the trend is large enough so that a precise estimate of the cooling effect cannot be given, but the uncertainty is small enough to know that there is a likely cooling effect from additional radiation reflected to space. Because of the break in the high-precision TOMS data record (May 1993 to July 1996), it is not currently known whether the reflectivity trend continued after 1992. The results emphasize the scientific importance of maintaining a high-precision long-term measurements program of key atmospheric parameters without data gaps.

When the least squares linear-fit trend is applied to each 1° × 1° scene, there are several distinct localized regions showing statistically significant changes in cloudiness. The most prominent of these is near the Antarctic ice shelf over the Weddell Sea with a small region showing increases of over 10 RU per decade (or 20% increase in reflectivity per decade). Over the ice shelf and the continent, there does not appear to have been any detectable change in reflectivity. The next largest region of reflectivity increase is near the west coast of Peru and Chile where the peak increase is about 6 RU per decade (25% increase per decade). There are two small regions of decrease in the Southern Hemisphere, over northern Australia and in the Pacific Ocean (27°S 155°W) with peak value of 3 RU per decade (about 14% decrease in reflectivity per decade).

Most of the regional changes in the Northern Hemisphere show decreases of about 3 to 6 RU per decade. These changes are northwestern United States and western Canada, 40°N (−3 to −6 RU per decade or −12 to −25% per decade), Europe, 45° to 55°N (−3 to −6 RU per decade or −10 to −15% per decade), eastern Russia, 58°N (−6 to −12% per decade), Korea (−6 to −12% per decade), and China 35°N, 85°E (about −10 to −20% per decade). Even though most of the smaller regional changes in the Northern Hemisphere (see Plate 2) are not statistically significant, the zonal averages show a statistically significant increase of about 0.5 RU per decade (see Figure 3) between 40°N and 60°N or about 1% per decade with larger changes occurring during the winter months (see Figure 5). The observed cloud changes are directly convertible into changes in UV radiation reaching the ground [Herman et al., 1999].

After removal of solar-cycle effects, zonal-average reflectivity increases at middle latitudes (30°–60°) yield small decadal decreases in UV-A (320–400 nm) of 1% per decade between 30° and 40°N and about 3% per decade between 40° and 60°N. For UV-B irradiance, 290–320 nm, the effects of cloud and ozone changes are partially offsetting so that predicted long-term UV-B increases would be smaller than previous estimates. For the 1980 to 1992 period the increases in zonal-average UV-B from all causes are unchanged from those estimated by Herman et al. [1996].

In the Northern Hemisphere the local regions of cloud reflectivity reduction over Europe, United States, Canada, Russia, and China represent corresponding regions of long-term UV irradiance increases in excess of that caused by ozone decreases. For example, erythral irradiance has about a 1-to-1 sensitivity to percentage changes in ozone and reflectivity (a 1% decrease in either ozone or cloud reflectivity produces a 1% increase in erythral irradiance [Herman et al., 1999]).

Appendix

Plate 3 shows the areas of significant cloud changes at high latitudes using the same trend data contained in Plate 2. Of interest are the large reflectivity increases indicated in the ocean areas surrounding the Antarctic continent, and smaller increases over the ocean areas near Alaska and northern Russia, and in the northern Atlantic Ocean. There are also small increases in reflectivity over the permanent Arctic ice sheet contrasted with no increases over the ice-covered Antarctic continent.

References

- Cavalalieri, D. J., P. Gloersen, C. L. Parkinson, J. C. Comiso, and H. J. Zwally, *Science*, 278, 1104–1106, 1997.
- Chiappello, I., J. R. Herman, J. Prospero, and C. Hsu, NIMBUS-7/TOMS detection of mineral dust over North Africa and Eastern North Atlantic Ocean, *J. Geophys. Res.*, 104, 9277–9291, 1999.
- Coakley, J. A., Jr., and P. Chylek, The two-stream approximation in radiative transfer: Including the angle of the incident radiation, *J. Atmos. Sci.*, 32, 409–418, 1975.
- Deirmendjian, D. *Electromagnetic Scattering on Spherical Polydispersions*, 290 pp., Elsevier, New York, 1969.
- Eck, T. F., P. K. Bhartia, P. H. Hwang, and L. L. Stowe, Reflectivity of Earth's surface and clouds in ultraviolet from satellite observations, *J. Geophys. Res.*, 92, 4287–4296, 1987.
- Eck, T. F., P. K. Bhartia, and J. B. Kerr, Satellite estimation of spectral UV-B irradiance using TOMS derived total ozone and UV reflectivity, *Geophys. Res. Lett.*, 22, 611–614, 1995.
- Harrison et al., *Atlas of Satellite Observations Related to Global Change*, edited by R. J. Gurney, J. L. Foster, and C. L. Parkinson, Cambridge Univ. Press, New York, 1993.
- Herman, J. R., and E. A. Celarier, Earth surface reflectivity climatology at 340 nm to 380 nm from TOMS data, *J. Geophys. Res.*, 102, 28,003–28,011, 1997.
- Herman, J. R., P. K. Bhartia, J. Ziemke, Z. Ahmad, and D. Larko, UV-B increases (1979–1992) from decreases on total ozone, *Geophys. Res. Lett.*, 23, 2117–2120, 1996.
- Herman, J. R., P. K. Bhartia, O. Torres, C. Hsu, C. Seftor, and E. Celarier, Global distribution of UV-absorbing aerosols from Nimbus-7/TOMS data, *J. Geophys. Res.*, 102, 16,911–16,922, 1997.
- Herman, J. R., N. Krotkov, E. Celarier, D. Larko, and G. Labow, The distribution of UV radiation at the Earth's surface from TOMS-measured UV-backscattered radiances, *J. Geophys. Res.*, 104, 12,059–12,076, 1999.
- Herman, J. R., E. Celarier, and D. Larko, UV 380 nm reflectivity of the Earth's surface, clouds, and aerosols, *J. Geophys. Res.*, in press, 2000.
- Hsu, N. C., J. R. Herman, O. Torres, B. N. Holben, D. Tanre, T. F. Eck, A. Smirnov, B. Chatenet, and F. Lavenu, Comparisons of the TOMS aerosol index with Sun photometer aerosol optical thickness, *J. Geophys. Res.*, 104, 6269–6279, 1999.
- Krotkov, N. A., P. K. Bhartia, J. R. Herman, V. Fioletov, and J. Kerr, Satellite estimation of spectral surface UV irradiance in the presence of tropospheric aerosols, 1, Cloud-free case, *J. Geophys. Res.*, 103, 8779–8793, 1998.
- Krotkov, N., J. R. Herman, P. K. Bhartia, Z. Ahmad, and V. Fioletov, Satellite estimation of spectral surface UV irradiance, 2, Effect of horizontally homogeneous clouds, *J. Geophys. Res.*, in press, 2000.
- Kuang, Z., Y. Jiang, and Y. Yung, Cloud optical thickness variations during 183–1991: Solar cycle or ENSO? *Geophys. Res. Lett.*, 25, 1415–1417, 1998.
- Lean, J. L., G. J. Rottman, H. L. Kyle, T. N. Woods, J. R. Hickey, and L. C. Puga, Detection and parameterization of variations in solar middle and near-ultraviolet radiation (200–400 nm), *J. Geophys. Res.*, 102, 29,939–29,956, 1997.
- Lubin, D., E. H. Jensen, and H. P. Gies, Global surface ultraviolet radiation climatology from TOMS and ERBE data, *J. Geophys. Res.*, 103, 26,061–26,092, 1998.
- Parkinson, C. L., D. J. Cavalalieri, P. Gloersen, H. J. Zwally, and J. C. Comiso, Arctic sea ice extents, areas, and trends, 1978–1996, *J. Geophys. Res.*, 104, 20,837–20,856, 1999.
- Stolarski, R. S., P. Bloomfield, R. D. McPeters, and J. R. Herman, Total ozone trends deduced from Nimbus 7 TOMS data, *Geophys. Res. Lett.*, 6, 1015–1018, 1991.

- Torres, O., P. K. Bhartia, J. R. Herman, and Z. Ahmad, Derivation of aerosol properties from satellite measurements of backscattered ultraviolet radiation, Theoretical basis, *J. Geophys. Res.*, **103**, 17,099–17,110, 1998.
- Ramanathan, V., and A. M. Vogelmann, Greenhouse effect, Atmospheric solar absorption, and the Earth's radiation budget: From the Arrhenius-Langley era to the 1990's, *Ambio*, **26**, 38–46, 1997.
- Willson, R. C., Solar irradiance, in *Atlas of Satellite Observations Related to Global Change*, edited by R. J. Gurney, J. L. Foster, and C. L. Parkinson, Cambridge Univ. Press, New York, 1993.
- Woods, T. N., et al., Validation of the UARS solar ultraviolet irradiances: Comparison with the ATLAS 1 and 2 measurements, *J. Geophys. Res.*, **101**, 9541–9569, 1996.
- Ziemke, J. R., S. Chandra, R. D. McPeters, and P. A. Newman, Dynamical proxies of column ozone with application to global trend models, *J. Geophys. Res.*, **102**, 6117–6129, 1997.
- J. R. Herman, Laboratory for Atmospheres, Goddard Space Flight Center, Code 916, Greenbelt, MD 20771. (herman@tparty.gsfc.nasa.gov)
- D. Larko, Raytheon STX Corporation, Lanham MD 20706.
- E. Celarier and J. Ziemke, SGT Inc., Greenbelt, MD 20770.

(Received June 11, 1999; revised April 7, 2000;
accepted April 13, 2000.)